


Article

Impact of Signalized Intersections on CO₂ and NO_x Emissions of Heavy Duty Vehicles

Nicolás Deschle ^{1,2,*} , Ernst Jan van Ark ¹, René van Gijlswijk ² and Robbert Janssen ²

- ¹ Sustainable Urban Mobility and Safety Group, Nederlandse Organisatie voor Toegepast Natuurwetenschappelijk Onderzoek (TNO), 2595 DA The Hague, The Netherlands; ernst_jan.vanark@tno.nl
- ² Sustainable Transport and Logistics Group, Nederlandse Organisatie voor Toegepast Natuurwetenschappelijk Onderzoek (TNO), 2595 DA The Hague, The Netherlands; rene.vangijlswijk@tno.nl (R.v.G.); robbert.janssen@transportbeat.nl (R.J.)
- * Correspondence: nico.deschle@tno.nl

Abstract: Pollutant emissions have been a topic of interest in the last decades. Not only environmentalists but also governments are taking rapid action to reduce emissions. As one of the main contributors, the transport sector is being subjected to strict scrutiny to ensure it complies with the short and long-term regulations. The measures imposed by governments clearly involve all the stakeholders in the logistics sector, from road authorities and logistic operators to truck manufacturers. The improvement of traffic conditions is one of the perspectives in which the reduction of emissions is being addressed. Optimization of traffic flow, avoidance of unnecessary stops, control of the cruise speed, and coordination of trips in an energy-efficient way are necessary steps to remain compliant with the upcoming regulations. In this study, we have estimated the CO₂ and NO_x emissions in heavy-duty vehicles while traversing signalized intersections, and we examined the differences between various behavioral scenarios. We found a consistent trend indicating that avoiding a stop can potentially reduce CO₂ and NO_x emissions by up to 0.32 kg and 1.8 g, respectively. Furthermore, an upper bound for the yearly CO₂ savings is provided for the case of the Netherlands. A reduction of 3.2% of the total CO₂ emitted by heavy-duty vehicles is estimated. These results put traffic control in the main scene as a yet unexplored dimension to control pollutant emissions, enabling authorities to more accurately estimate cost–benefit plans for traffic control system investments.

Keywords: sustainable transport; emissions; fuel consumption; connected transport; intelligent transport systems; energy efficiency



Citation: Deschle, N.; van Ark, E. J.; van Gijlswijk, R.; Janssen, R. Impact of Signalized Intersections on CO₂ and NO_x Emissions of Heavy Duty Vehicles. *Energies* **2022**, *15*, 1242.

<https://doi.org/10.3390/en15031242>

Academic Editors: Michail Makridis, Hesham A. Rakha and Georgios Fontaras

Received: 18 December 2021

Accepted: 15 January 2022

Published: 8 February 2022

Publisher's Note: MDPI stays neutral with regard to jurisdictional claims in published maps and institutional affiliations.



Copyright: © 2022 by the authors. Licensee MDPI, Basel, Switzerland. This article is an open access article distributed under the terms and conditions of the Creative Commons Attribution (CC BY) license (<https://creativecommons.org/licenses/by/4.0/>).

1. Introduction

Despite tremendous improvements in recent years, world air quality is still far from the levels that do not represent a risk for human health and the environment. Nitrogen oxides (NO_x), together with particulate matter, ground level ozone (O₃), and ammonia (NH₃), are among the most problematic air pollutants [1–6]. At the same time, the concentration of greenhouse gases such as CO₂ keep increasing in the atmosphere. Road transportation is not only one of the main causes of NO_x and CO₂ emissions, but it is also the main factor in the logistic costs. Furthermore, a high percentage of these emissions occurs in specific corridors where most of the freight traffic takes place. Reducing the emissions and fuel usage in these specific corridors can have a huge economic and environmental impact.

1.1. Fuel Consumption, CO₂ and NO_x Emissions

Depending on the degree of development of the country, domestic logistics costs account for 5% to 20% of a country's gross domestic product (GDP), of which about 60% are transportation costs [7,8]. Although the global road to rail modal split ratio is estimated to be 60:40, this varies significantly from one country to another. Specifically, in Latin America and China, the percentage of rail transport is below 25%, and it is under 40% for the United

States (US) [9]. The European Union (EU) is more heterogeneous; the estimations of the road–rail modal split vary from 17% [10] to 34% [9]. Rail dominates in a few countries that share certain characteristics, i.e., span large areas with very irregular population distribution as Australia, Russia and Canada. Furthermore, in the last 10 years, the share of road freight activity showed to be increasing with respect to rail freight worldwide [9].

At the same time, the transport industry is a significant source of NO_x emission, as well as greenhouse gases such as CO₂. As of 2015, the transportation sector was responsible for 7% of the total CO₂ energy-related emissions [9]. In the EU, transportation overall is responsible for 14% of CO₂ emissions, as well as a main contributor to the overall NO_x emissions [11]. Road and rail transport emissions together account for 32% of the total NO_x of the US [12,13], and vehicle emissions altogether have been found to be the major contributor to roadside NO_x pollution [14]. Furthermore, freight transport, which is highly dominated by trucks, constitutes 25% of the US's total CO₂ emissions [12,15]. Altogether, these figures call for urgent action in road transportation in order to let the logistics expand, allowing for economic growth with a smaller impact on air quality as described in the emissions goals in particular in the EU.

The last two decades have already shown a shift in freight transport research towards sustainability and safety affecting heavy-duty transport vehicles in a number of ways. Different options have been and are being explored at different levels, ranging from exploring different energy sources to automation and coordination. The changes in the transport of goods could be classified as follows; vehicle energy consumption and efficiency, control of emissions, and, finally, automation and coordination, both between vehicles and with the network infrastructure.

1.2. Transport Corridors

Special attention must be given to the main corridors, where a high percentage of heavy-duty transport takes place. These corridors are also known for playing a critical role in the expansion economy [16]. Roberts and coworkers found that although the economic benefits are significant, large transport infrastructure projects can detrimentally impact the environment. Clearly, focusing on these specific routes is key to have a high impact on overall transport. It is in this context that in 2009, the EU started the development of the Trans-European Transport Network (TEN-T), which aims to improve the European transport network focused to allow sustainable growth of the economy with special attention on the identified nine *Core Network Corridors* [17–20], of which 39% of the road corridors are off highways [21]. Projects at national level also support these initiatives, as are the cases of the *top corridors* program and the *Connected Transport Corridors* consortium [22] in The Netherlands, which aim to scale up the currently available technology in four main Dutch corridors in order to achieve a more efficient, sustainable, and safe transport of goods. In particular, one of the objectives is the implementation and analysis of coordination systems between the vehicles and the infrastructure.

1.3. Emissions and Traffic Control

Reducing the number of stops of vehicles can lead to a drop in travel time, fuel consumption, and undesired emissions (CO₂, NO_x); at the same time, that increases the safety on road (see [23] and the references therein, for example, ref. [24]). Although initially aimed to reduce travel time rather than increase sustainability, methods to maintain a steady flow in main roads have been around since the implementation of the green waves studied since the late 1910s [25,26]. Further steps in this direction were green waves influenced by induction loops where the fixed or manually adjustable schedule was replaced by a dynamic algorithm with the traffic flow on specific points as input. The application of induction loops for traffic control was introduced in the 1960s [27] and has been under development since then. Some of the currently widely used traffic control systems based on induction loops are SCOOT [28] and SCAT [29]. In the Netherlands, the VECOM and VETAG systems have been in use since the 1970s [30–32]. Since then, diverse efforts

have been put into developing communication systems between vehicles, infrastructure, and traffic management centers. This technology is now widely referred to as intelligent transport systems (ITS). PROMETHEUS, probably the first European research program on ITS, dates back to the 1980s [33]. It was around the same time that the Interstate Surface Transportation Efficiency Act (ISTEA) in the US issued the theme of ITS ([34] p. 625). In the early 2000s, the ubiquitous availability of Global Positioning System (GPS) devices and wireless communication boosted ITS technology developing *Cooperative-ITS* (C-ITS) systems, among which intelligent traffic light control systems (iTLC) can be found. iTLCs not only receive information about traffic in advance both from induction loops and from cell-phone applications, allowing the coordination of traffic, reducing the number of stops, but these systems also communicate bidirectionally, sending back information to the vehicle or the driver and being able to concede priority and determine the optimal speed based on real-time data. iTLC systems come with a great opportunity since they can contribute to achieving the environmental goals by optimizing traffic so that emissions are minimized.

1.4. Previous Studies

Several projects in the last decade have addressed the impact of the interaction between traffic control and behavior on pollutant emissions. Despite most of these studies aiming to bridge the gap between laboratory tests (as those performed on a dynamometer) and real-world emissions, very few of them involve real-world field measurements. Much research is focused on theoretical optimization such as determining optimal speed in terms of CO₂ and NO_x [35,36] or under the relation between emissions on different traffic conditions based on the level of urbanization. In 2017, Wang and Rakha developed a model to determine real-world optimal accelerations and cruise speed for heavy-duty vehicles (HDV) [36]. Guardiola and co-workers studied the NO_x emissions on passenger cars when approaching a traffic light using three modeled speed profiles measured on a chassis, finding savings in the range of 7.5–12% and 13–32% for fuel emissions and NO_x, respectively [37]. Real-world measurements were conducted by Meneguzzo et al. comparing NO_x and CO₂ emissions on passenger cars on a route where traffic lights had been replaced by a roundabout [38]. Several European projects measured fuel consumption differences under traffic control measures. The Freilot project, which is probably the largest project to date with measurements on 177 trucks over 12 months around Europe, reported savings up to 13% in fuel consumption on HDVs by means of energy efficient intersection control [39], followed by Compass4D, where 45 trucks with C-ITS capabilities (priority and speed advice) were measured and fuel savings in the order of 20–60 g per km were found [40,41].

Despite the vast evidence supporting the potential of traffic control systems to reduce emissions, the heterogeneity of the methods and relatively limited published results make the comparison and scale up of these results very involved. Moreover, although both are deeply valuable to have a proper assessment of the vehicle emissions, it has been made evident the need for in-vehicle methods in addition to the lab ones. The former ones allow incorporating the diverse dependencies that are in play, tackling the problem as the real multivariate problem that it is [42].

An accurate and clean figure obtained from real-world measurements is still missing, and helping to fill that gap is the goal of this paper. By means of an in-vehicle measurement unit, we estimated the emissions of HDV performing their normal operations during a long period of time and on different roads. The data were processed to link it to the road network in order to make possible to systematically extract all the segments of the trajectories around signalized intersections. This is—to our knowledge—the first study of this kind where real-world emissions, including the whole spectrum of dependencies such as traffic conditions and driving behavior, were investigated over a dataset of several months long. Furthermore, thanks to the size of the dataset, we provided an outcome statistically sound that allows for scaling up to determine the impact on a larger scale.

2. Materials and Methods

In the present work we studied the effect that the change in behavior caused by traffic lights have in emissions of CO₂ and NO_x in HDV. For that purpose, we determined the total mass of CO₂ and NO_x emitted by vehicles over a fixed distance around different intersection crossings, and we further classified these passages based on their behavior in three groups: no-stop, slow-down, and stop. The three different behaviors identified were used to define the sampled groups. Under the assumption that all the crossings are independent from each other, we performed a statistical test to determine whether the differences of the level of emissions among the three groups are different on the population (please refer to the end on Section 2.4 to see the tests used and to the Appendix A.2 for further details). Furthermore, we conducted an in-depth qualitative analysis of the CO₂ and NO_x time series for the different groups. As a global observable of the time series of each group, we used the median to obtain a smoother and less outlier-sensitive measure. The time series were analyzed together with the vehicle behavior. Finally, using the CO₂ differences between groups, we estimated the impact of these savings on the Dutch population. To do so, we estimated the number of intersections that an HDV encounters per unit of distance, and the probability of the passages to belong to each of the three behavioral groups are described in this work using large amounts of collected data.

Data from a group of five vehicles conducting normal operations in The Netherlands were used. From these vehicles, time series for GPS, speed, CO₂, and NO_x have been logged for their entire routes. Since we are interested only in the segments around signalized intersection passages, we first identified the location of the traffic lights in The Netherlands. Next, the data around the crossing were selected from the entire trajectory to study the different speed and emission profiles and, in particular, the differences in emissions of different approaches. Furthermore, the data were subjected to a process of filtering, analysis, and enrichment. The following subsections are dedicated to explaining: first, the physical measurements and the properties of the vehicles employed; second, the pre-processing and enrichment of the data acquired; and third, the analysis, which includes filtering and reference to the statistical methods used.

2.1. Physical Measurements and Data Acquisition

The measurements were conducted on five Euro VI DAF trucks with engines with power between 315 and 355 kW (see Table 1 for details). These data were acquired in the context of the integrator project [43] and were made available for this study. The total weight of the vehicles was also estimated by means of the truck features and their kinematics over all the datasets. The mean and standard deviation of the total mass (tractor + load) of the vehicles including all the trips were 25.75 t and 9.05 t, respectively. This was estimated for each trip as described in the Appendix A. The data were acquired between September 2019 and February 2020, while the trucks realized their normal operations in The Netherlands region, traversing a total of 230,000 km. Although the routes included segments outside The Netherlands, only the segments conducted on the Dutch Network were used in this analysis.

Table 1. Details of all the vehicles included in the study. They were DAF trucks with similar characteristics. The rated power was between 320 and 355 kW.

Engine	Power [kW]
XF 440 FTG	320
XF 460 FTG	341
XF 440 FT	324
XF 480 FTG	353
XF 480 MX-13	355

SEMS System

Onboard measurements were conducted by means of the *Smart Emissions Measurement System* (SEMS) developed by TNO. This system provides a simple and easy-to-use, yet robust and reliable emissions monitoring solution. It has been tested extensively since its development in 2012 (see for example, refs. [44–46]), and there is an ongoing project to develop its industrialization and large-scale deployment [47]. A series of measurement systems needs to be installed on the vehicles, whereas some data have been obtained from devices already installed by the original manufacturer.

The first group encompasses a GPS receiver as well as sensors to then estimate NO_x , O_2 , and NH_3 concentrations and exhaust gas temperature. The sensors were mounted near the end of the exhaust line, in threaded bushes welded through the wall of the tailpipe. Regarding the second group, data from the CAN-bus were acquired, such as velocity, throttle position, and rotational speed of the engine.

The NO_x massflow and CO_2 massflow were calculated by combining sensor signals and CAN-bus signals. First, the exhaust massflow was calculated by summing air massflow and fuel massflow. Air massflow and fuel volume flow were available on the CAN-bus of each of the vehicles in this study. The fuel density is an assumption: 835 g L^{-1} . The NO_x massflow was calculated by multiplying the exhaust massflow with the NO_x concentration (calibrated, corrected for NH_3). The CO_2 massflow was calculated by multiplying the fuel massflow by a fuel specific CO_2 emission factor, in this case, $3.15 \text{ CO}_2/\text{diesel}$.

All data were sampled once per second and gathered in a data logger located in the cabin, as depicted in Figure 1. This small computer was set up to start (stop) acquisition when the ignition was turned on (off). A built-in data transmitter periodically uploaded the data to a server. A computer running a scheduled preprocessing task picked up the data from the server, performed checks, corrections, and calculations on the data (see Section 2.2.1) and wrote it in a dedicated SEMS database.

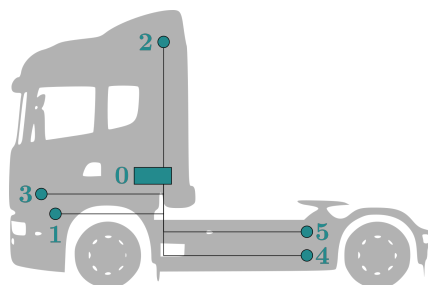


Figure 1. Diagram of a tractor with the location of the different measuring systems installed on the vehicle depicted in green. (1) CAN-bus sensor, (2) GPS antenna, (3) Air pressure sensor, (4) Temperature sensor, and (5) Exhaust sensors of NO_x and O_2 . (0) Indicates the location of the onboard unit system responsible for logging the data.

2.2. Data Processing

2.2.1. SEMS Preprocessing

Data as collected from sensors generally need preprocessing to remove illogical values and spikes that cannot be explained by the conditions. Furthermore, some signals require calibration-based corrections. The variation in the CAN-bus signal implementation among manufacturers is another reason to perform checks and corrections. The preprocessing of the SEMS data is performed automatically on a server, although some preemptive checks have been already performed within the SEMS itself. The following tasks are performed during preprocessing:

- Calibration: Sensor data are corrected using a function based on calibration of the particular sensor in the lab;
- Speed signals from GPS and vehicles are compared and combined to produce a good and continuous signal;

- Raw cleaning: check for negative values, filter some signals for spikes, remove signals when the engine is not running, and fill small gaps in the data if possible;
- Time alignment: align signals related to emissions to signals related to the engine;
- Ammonia correction: correction of NO_x concentration signal for ammonia, based on ammonia sensor values. This is necessary because the NO_x sensor is cross sensitive for NH₃;
- Mass flow calculation: Emissions in grams are calculated by calculating the flow of exhaust gas and multiplying it with the concentrations observed.

The result is a set of clean 1 Hz signals that can be used for further calculations, e.g., of emissions per km.

2.2.2. Data Enrichment and Selection

In order to enrich the data with information from the infrastructure, the time series of the GPS data needed to be connected to the road network. For each trip, then, the trajectory was *map-matched* using the *Open Source Routing Machine* (OSRM) [48]. The result of this is a new time series where each point is a node on *Open Street Maps* (OSM) [49] from where any information present on it can be added to the original data.

Once the data were linked to the map, we could identify all the points in the data in which a vehicle is crossing a signalized traffic light (based on traffic light locations as in OSM) and the respective segment of the road of equal length before and after the intersection. We identified the start and end points of segments of 2 km length centered on the intersection crossing and also the vehicle action on the intersection. i.e., the maneuver. Acknowledgedly arbitrarily, 1000 m has been chosen based on the typical deceleration of a heavy-duty vehicle that can take up to 1 km [50,51]. From the original data, the time series between the segment's start and end were retrieved; this process is schematized in Figure 2. The result is a series of N intersection passages p_i defining a set $P = \{p_1, \dots, p_N\}$. Each of these passages d_i consists of a group of time series of equal length representing the position ($x_i(t)$), the velocity ($v_i(t)$), and the instantaneous CO₂ and NO_x mass flow ($\xi_i(t)$ and $\theta_i(t)$), plus the maneuver taken by the vehicle (straight, right/left turn, u-turn) represented by m_i , i.e., $p_i = (x_i(t), v_i(t), \xi_i(t), \theta_i(t), m_i)$. The number of passages obtained was $N = 11,087$, from which only those with straight maneuver were picked, resulting in a smaller set $\tilde{P} = \{p_i \in P \mid m_i = \text{straight}\}$ with $|\tilde{P}| = 4972$. Provided the correlation between turn radius and vehicle's velocity, the analysis of the turns is significantly more demanding and the interpretation of the results cumbersome; hence, it was not carried out in this work and remains to be explored in future research.

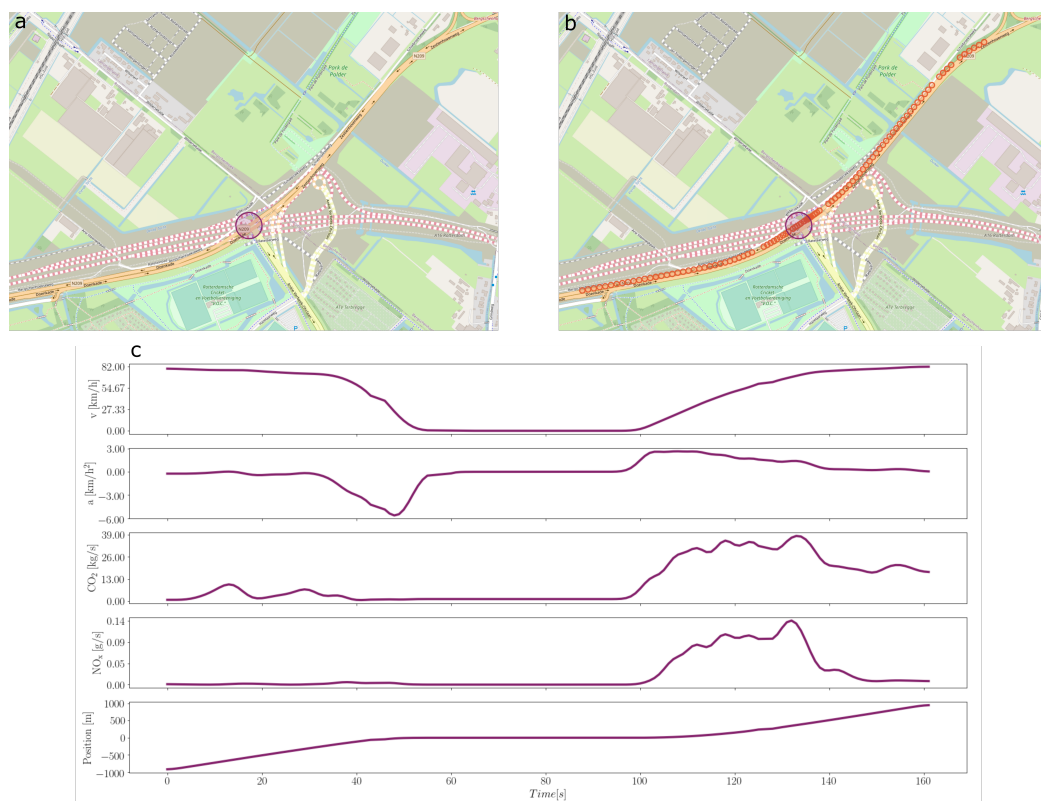


Figure 2. Example of the extraction of the data around the intersections. (a) Signalized intersections were identified on the map. (b) The fragment of length 2 km symmetric around the intersection was selected based on the position data. (c) All the time series relevant for this study were gathered; from top to bottom, the velocity, acceleration, instantaneous CO_2 , and the instantaneous NO_x . At the bottom, the position of the vehicle relative to the stop line is plotted for reference. There is a period between 60 to 100 s in which the vehicle is waiting at the traffic light. Around 100 s is when the vehicle starts moving. Data spans only until the vehicle is 1000 m past the intersection.

2.3. Analysis

2.3.1. Clustering

Three different clusters were defined from the speed profiles with a set of simple rules. These clusters represent different scenarios to be analyzed: a scenario in which the vehicle does not stop at the intersection and does not change its speed significantly; a scenario in which the vehicle has to stop completely at the intersection; and an intermediate scenario in which the vehicle decreases its speed significantly before the intersection but does not stop. Throughout the rest of the paper, we refer to these clusters as no-stop, stop, and slow-down, and we associate them with the colors green, red, and amber, respectively. The clusters are based on the mean velocity of the vehicle in two main subsegments, the immediate last 600 m before the intersection and the 400 m that are between 1000 m and 600 m from the intersection. Defining for each passage i the mean velocity of the subsegment determined by the interval $\psi = (a, b)$ as:

$$\bar{v}_i^\psi = \int_\psi dt v_i(t) = \int_a^b dt v_i(t), \quad (1)$$

we have defined the mean velocities over five subsegments of interest. First, the three mean velocities \bar{v}_i^α , \bar{v}_i^β , and \bar{v}_i^γ for intervals $\alpha = [-600, -400)$ m, $\beta = [-400, -200)$ m, and $\gamma = [-200, 50)$ m, respectively, are the three intervals used to classify the clusters. Two additional mean speeds, \bar{v}_i^ρ , \bar{v}_i^ω for $\rho = [-1000, -600)$ m, $\omega = [50, 1000)$ m, over the remaining parts of the passage were used to homogenize the behavior farther from the intersection. The same conditions are defined for the mean velocities \bar{v}_i^ρ , \bar{v}_i^ω for the

three clusters. This reduces the general variability caused by external conditions such as traffic or weather. The three clusters are then defined based on a set of rules over \bar{v}_i^ϵ with $\epsilon \in \{\alpha, \beta, \gamma, \rho, \omega\}$ as follows:

$$\begin{aligned}
 C_{\text{no-stop}} &= \{i \in P \mid \bar{v}_i^\rho > 60 \text{ km/h} \wedge \bar{v}_i^\epsilon > 60 \text{ km/h} \forall \epsilon \in \{\alpha, \beta, \gamma\} \\
 &\quad \wedge \bar{v}_i^\omega > 30 \text{ km/h} \wedge \nexists t \in [-1000, 1000] \mid v_i(t) < 3 \text{ km/h}\}, \\
 C_{\text{slow-down}} &= \{i \in P \mid \bar{v}_i^\rho > 60 \text{ km/h} \wedge \bar{v}_i^\epsilon > 30 \text{ km/h} \forall \epsilon \in \{\alpha, \beta, \gamma\} \\
 &\quad \wedge \exists \epsilon' \mid \epsilon' \in \{\alpha, \beta, \gamma\} \wedge \bar{v}_i^{\epsilon'} < \bar{v}_i^\rho \wedge \bar{v}_i^\omega > 30 \text{ km/h} \\
 &\quad \wedge \nexists t \in [-1000, 1000] \mid v_i(t) < 3 \text{ km/h}\}, \\
 C_{\text{stop}} &= \{i \in P \mid \bar{v}_i^\rho > 60 \text{ km/h} \wedge \bar{v}_i^\omega > 30 \text{ km/h} \\
 &\quad \wedge \exists t \in \alpha \cup \beta \cup \gamma \mid v_i(t) < 3 \text{ km/h} \wedge \nexists t \in \rho \cup \omega \mid v_i(t) < 3 \text{ km/h}\},
 \end{aligned}
 \tag{2}$$

These rules define the disjoint sets $C_{\text{no-stop}}$, $C_{\text{slow-down}}$, and C_{stop} that do not necessarily span the set of all the intersection passages, i.e., $C_{\text{no-stop}} \cup C_{\text{slow-down}} \cup C_{\text{stop}} \subseteq C$. The results of the classification of the 4096 trajectories in $|\bar{P}|$ are shown in Table 2. A detailed graphical representation of the rules that defined the cluster is shown in Figure 3.

Table 2. Number of passages classified in each of the three clusters after analyzing the $|\bar{P}| = 4096$ straight passages. It can be noted that the sum of the passages over the three clusters does not add to 4096 because not all the passages belong to a cluster.

Cluster	Number of Passages
no-stop	378
slow-down	349
stop	175

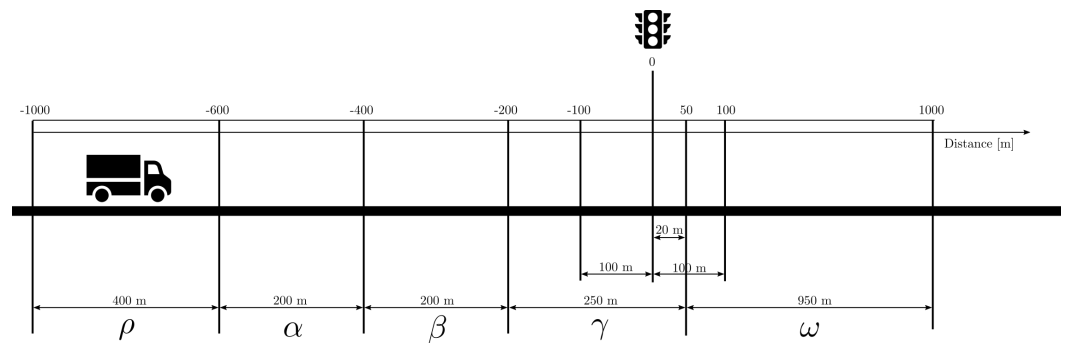


Figure 3. Details of the set of rules used in the study to determine the three clusters. The rules are mainly based on the approach to the intersection, and they are significantly laxer on the conditions of the velocity after the intersection. In all cases, the vehicle mean velocity over the immediate 400 m segment 600 m away from the intersection is greater than 60 km/h. The 600 m prior to the intersection is where the clusters are distinguished; for the no-stop case, the mean velocity is greater than 60 km/h over the whole 600 m segment. For the stop cluster, the vehicle stops completely (the velocity vanishes) at least once in the segment. Finally, for the slow-down cluster, the mean velocity is lower than the mean velocity on the previous segment but greater than 30 km/h, and furthermore, the instantaneous velocity is greater than 30 km/h. The mean velocity over the 1000 m after the intersection for the vehicles in all the clusters needs to be greater than 30 km/h.

2.4. Outcome Measures

For all the intersection passages to be used in the analysis, the total CO₂ and NO_x over each 2 km segment was computed by integrating the instantaneous quantities $\zeta_i(t)$ and $\theta_i(t)$:

$$\Xi_i = \int_{s_i} dt \zeta_i(t) \text{ for } i = 1 \dots N, \quad (3)$$

and

$$\Theta_i = \int_{s_i} dt \theta_i(t) \text{ for } i = 1 \dots N, \quad (4)$$

where the lower case $\zeta_i(t)$ and $\theta_i(t)$ are time-dependent quantities of passage i and represent the instantaneous CO₂ and NO_x concentrations at the tail-pipe, respectively; s_i is the total time interval that it takes the vehicle i to transverse the entire 2 km passage; N is the total number of passages included in the analysis; and the upper case Ξ_i and Θ_i state the accumulated CO₂ and NO_x emitted over the entire intersection passage i , respectively.

Once Ξ_i and Θ_i for all passages i are computed, they are grouped by the clusters defined using the speed profiles (Equation (2)) as follows:

$$\begin{aligned} \hat{\Xi}_j &= \{\Xi_i | i \in C_j\} \\ \hat{\Theta}_j &= \{\Theta_i | i \in C_j\}, \end{aligned} \quad (5)$$

for $j \in \{\text{no-stop, slow-down, stop}\}$. These are the six sets we analyzed (two outcome measures for three groups). The mean emissions for each group are then defined as:

$$\begin{aligned} \langle \hat{\Xi}_j \rangle &= \frac{1}{N_j} \sum_{i=1}^{N_j} \Xi_i \text{ with } N_j = |\hat{\Xi}_j| \\ \langle \hat{\Theta}_j \rangle &= \frac{1}{N_j} \sum_{i=1}^{N_j} \Theta_i \text{ with } N_j = |\hat{\Theta}_j| \end{aligned} \quad (6)$$

To determine whether the observed differences in the sample hold for the population, we performed a statistical significance analysis over $\hat{\Theta}_j$ and $\hat{\Xi}_j$, for $j \in \{\text{no-stop, slow-down, stop}\}$. Provided that the data are not normally distributed, the statistical significance of the results was assessed by means of a Kruskal–Wallis Rank test followed by a Pairwise Dunn test to determine the significance between the groups. For the behavioral analysis and visualization of the time series, the instantaneous median of the emissions for CO₂ and NO_x and the speed were computed for each group as follows:

$$\begin{aligned} \zeta'_j(t) &= \text{med}\{\zeta_i | i \in C_i\} \\ \theta'_j(t) &= \text{med}\{\theta_i | i \in C_i\} \\ v'_j(t) &= \text{med}\{v_i | i \in C_i\}, \end{aligned} \quad (7)$$

where $\text{med}\{\cdot\}$ stands for the median. This is used as a proxy for the overall instantaneous behavior of each group.

2.5. Impact

To analyze the impact of the intersection passages on energy efficiency it is necessary to estimate the frequency of these events. In order to do this, we analyzed the behavior of 51 different HDV driving in the Netherlands. First, we determined the expectation value for n : the number of intersections encountered per km of road for each trip:

$$\mathbb{E}[n] = \frac{1}{N_T} \sum_i^{N_T} \frac{N_i}{l_i}, \quad (8)$$

where l_i is the distance of the i -th trip (in km), N_i is the number of intersections found in trip i , and N_T is the total number of trips. Combining this value with s , the total yearly distance driven as reported by the Dutch Central Bureau for Statistics (CBS) [52]; the total number of intersection passages for the entire HDV fleet in The Netherlands can be calculated as follows: $s \cdot \mathbb{E}[n]$. Next, identifying how often each passage behavior falls into one of the three clusters defined in Section 2.3.1, we determined the probability p_i with $i \in \{\text{no-stop, slow-down, stop}\}$ with which the three behaviors (no-stop, slow-down, stop) occur at an intersection. Finally, the upper bound for the savings, Δ —corresponding to the case in which all the stops and slow-down cases can be avoided completely—can be estimated via:

$$\Delta = s \cdot \mathbb{E}[n](p_{\text{stop}} \cdot \Delta_{\text{stop,no-stop}} + p_{\text{slow-down}} \cdot \Delta_{\text{slow-down,no-stop}}), \quad (9)$$

where $\Delta_{i,j}$ is the median difference in CO₂ emitted between clusters i and j , or, more explicitly:

$$\Delta_{i,j} = \text{med}\{\hat{\mathbb{E}}_i, \hat{\mathbb{E}}_j\} \quad (10)$$

3. Results

In this section we present the results of the analysis done following the methodology explained in Section 2. In the first subsection we analyze the speed profiles for the different clusters before presenting the emission analysis. This is done by computing the instantaneous median speed over each cluster (Equation (7)) and is shown in Figure 4. In the following two subsections, we present the results of the emissions in the crossings for CO₂ and NO_x, respectively. For CO₂, the median instantaneous CO₂ computed following (7) and the total emissions for each passage calculated as in (10) for each cluster separately are shown in Figure 5a,b. The distribution of the total CO₂ emitted for all vehicles, including those that do not belong in any of the clusters is shown in Figure 6. Analogously for NO_x, Figure 7a,b show the results obtained by means of Equations (7) and (10), respectively. Figure 8a,b, show the cumulative levels for CO₂ and NO_x along the passages. Finally, Figure 9 shows the results for the scaling up of the results to a whole year in The Netherlands.

3.1. Clustering of the Speed Profiles

The results of the clustering are shown in Figure 4. The solid lines represent the median speed of each cluster along the 2000 m segment, $v'_j(t)$ (see Equation (7)), whereas the shaded areas signify the standard deviation. In green, the no-stop cluster seems to keep a constant speed with relatively small deviation, while in amber, the slow-down cluster decreases its speed when approaching the intersection but does not stop. Finally, on the median of the stop cluster, it can be observed that the speed of the vehicles decreases significantly at the intersection. The reason why the median does not vanish is because not all the vehicles stop exactly at 0 m; instead, because of queues, many vehicles stop before it. It is also worth noticing that the standard deviations for all the clusters are smaller on the approach than after the intersection. This can be explained by the way the clusters are defined, where the rules apply to the approach and not to the segment after the intersection. The final speeds of the clusters then also differ, which we address in Section 4.

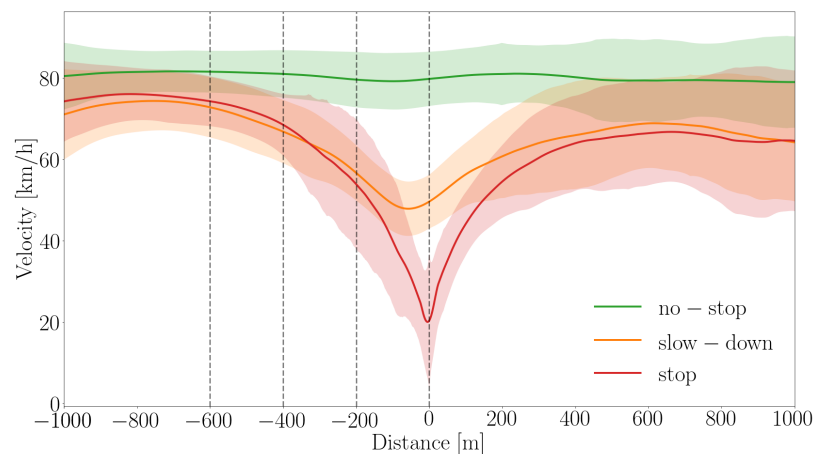


Figure 4. Speed profiles for the three different groups. The median instantaneous speed ($v'_j(t)$, see Equation (7)) of each of the three groups; no-stop, slow-down, and stop in green, amber, and red, respectively. The shaded areas indicate the instantaneous standard deviation for each of the groups.

3.2. CO₂ Emissions

Figure 5a shows the median instantaneous CO₂ flow over the entire 2 km passage, that is, $\zeta'_j(t)$, computed as indicated in Equation (7). As expected, the slopes of the stop and slow-down clusters (in red and amber) right after the intersection are similar; in both cases, the vehicles accelerate full-throttle after the intersection. Since the vehicles in the slow-down cluster have a higher initial speed, the period of full throttle is shorter, and the peak of this cluster is lower. Finally, the green curve represents the no-stop cluster. Its median, although fairly more stable than those of the other two clusters, is not as flat as one could have expected, which is further discussed in Section 4. In Figure 5b, we present box plots for the distribution of the total CO₂ for each of the clusters over the entire 2 km passage, that is, the integral of the CO₂ along the passage, which is computed as indicated in Equation (10). The largest differences emerge in the stop cluster compared to any of the other two clusters. The differences with the stop group are statistically significant. The difference in CO₂ emissions between the stop and no-stop is 0.32 kg, which translates into 0.12 L of diesel fuel. As can be seen in Figures 5 and 8a, when reaching the intersection, the CO₂ levels emitted by the no-stop subpopulation are near constant, hence its cumulative levels are linear, which, at the intersection, are higher than the other two which were coasting in this segment preceding the stop line. Furthermore, the stop cluster reaches the intersection with the lowest values, and this enhances the impact of the stop and subsequent throttle: 100 m after the intersection, the cumulative CO₂ values from the stop cluster are already higher than the other two. At the end of the segment, the slow down cluster is smaller than the no-stop cluster, which seems to indicate that slowing down is more energy efficient than not doing it. This can also be observed in Figure 8 where the value of the slow-down cluster is smaller than the no-stop cluster. The difference between these two clusters is slim, and several points need to be taken into account. The final velocities of the clusters are not the same (see Figure 4); instead, the final median velocity of the no-stop cluster is higher than the other two. This might indicate that the segment length chosen is too short for HDVs, that they have not reached their target speeds after 1 km beyond the intersection, and that the CO₂ of the stop and slow-down is being underestimated. In addition, this does not hold for the median, which might also indicate that the means are affected by outliers. Furthermore, the definition of the clusters is very clear for the stop and no-stop clusters, whereas the definition of the slow down behavior is more delicate and may well require further fine tuning. Figure 6 shows the distribution of the total CO₂ emitted per passage, i.e., Ξ_i for $i \in N$, the total number of passages used in the study (see Equation (3)). The distribution is not symmetric, indicating that there are passages with

higher emissions than the ones in the groups defined in this work. We will address the consequences of this in Section 4.

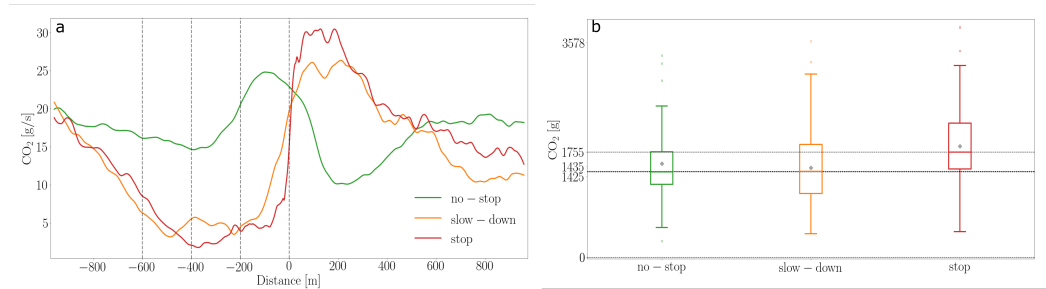


Figure 5. (a) Median instantaneous CO₂ flow for the three groups. Green, amber, and red represent the no-stop, slow-down, and stop groups, respectively. Position is relative to the location of the intersection as described on OSM. Vertical dashed lines denote the different regions used to group the speed profiles (see Section 2). (b) Results for the CO₂ flow for the three groups. Green, amber, and red represent the no-stop, slow-down, and stop groups, respectively. Differences between all groups are significant.

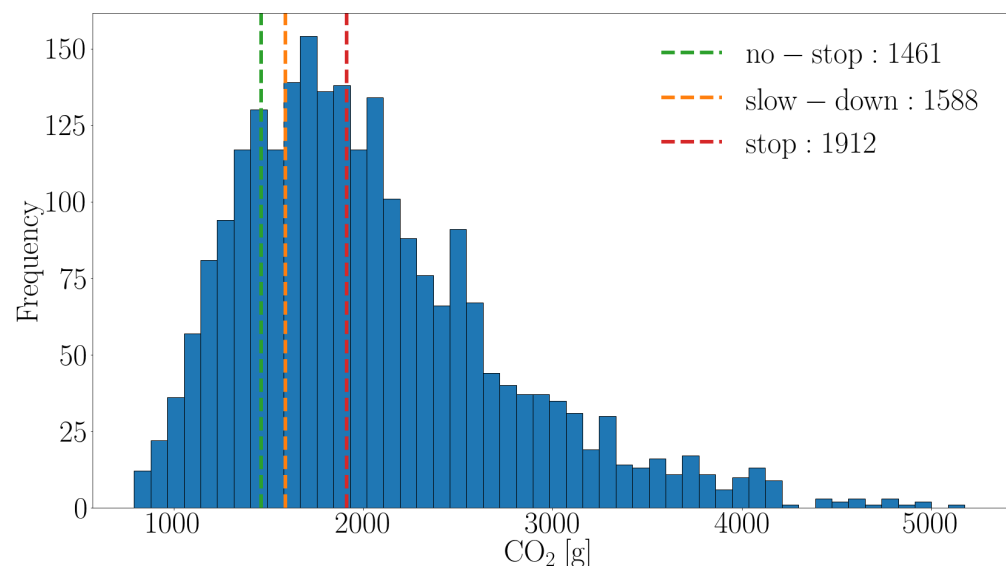


Figure 6. Distribution of the CO₂ emitted on the 2 km passage. In green, amber, and red the median values for the no-stop, slow-down, and stop clusters, respectively. The distribution is skewed, and many values of emitted CO₂ occur when interaction with other factors such as traffic is present. This indicates that the gap between the no-stopping vehicle and a vehicle that stops can increase.

3.3. NO_x Emissions

The median instantaneous NO_x emissions, $\theta'_j(t)$ for $j \in \{\text{no-stop, slow-down, stop}\}$ (Equation (7)) together with the medians of the total NO_x emissions per passage, $\hat{\Theta}_j$ (Equation (5)), are depicted in Figure 7. The three clusters have very differentiated levels of NO_x with a clear negative impact of the stop on the NO_x levels (see Figure 7a). As with the CO₂, the NO_x levels are related to the acceleration and throttle pattern after the intersection, but contrary to that case, the NO_x levels for the stop and slow-down are clearly distinguishable. As can be seen from the total median NO_x emissions (Figure 7), the stop population emits more than five times the same NO_x in the 2 km passage than the slow-down cluster. It is of main interest to contrast these values to the current regulations, in particular, those applying to the location of the measurements in the EU. As a reference, the current NO_x emission limit for vehicles in the category Euro VI is 0.46 g/kWh [53,54], which, for a typical HDV, could be roughly translated into 0.5 g/km of NO_x (assuming

an average truck demand of 1.1 kW h/km). Figure 8b shows a different story for the NO_x compared to the CO₂. All changes in velocity are associated with an increase in the NO_x levels. The cumulative NO_x emitted by the no-stop cluster is never higher than that of the other two. Looking at the segment before the intersection, in which the slow-down cluster holds a lower speed, it can be interpreted that holding a lower constant speed is associated with higher NO_x levels. Moreover, after the intersection, the longer full throttle from the stop cluster raises its cumulative value that overtakes the slow-down cluster 200 m after the intersection.

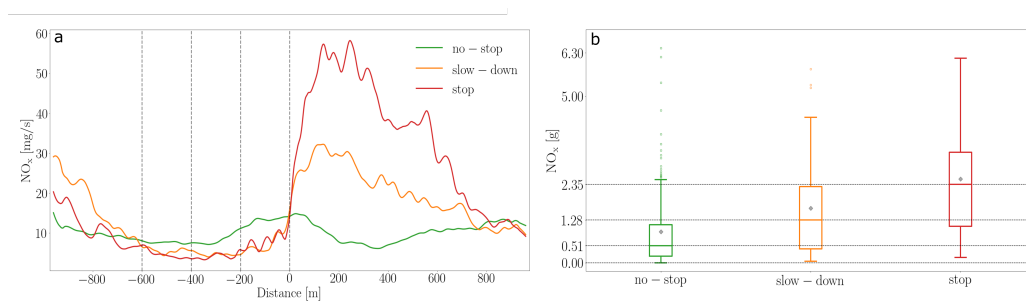


Figure 7. (a) Median instantaneous NO_x flow for the three groups. Green, amber, and red represent the no-stop, slow-down, and stop groups, respectively. The position is relative to the location of the intersection, as described on OSM. The vertical dashed lines denote the different regions used to group the speed profiles (see Section 2 for further details). (b) Results for the NO_x flow for the three groups. Green, amber, and red represent the no-stop, slow-down, and stop groups, respectively. Differences between all groups are significant.

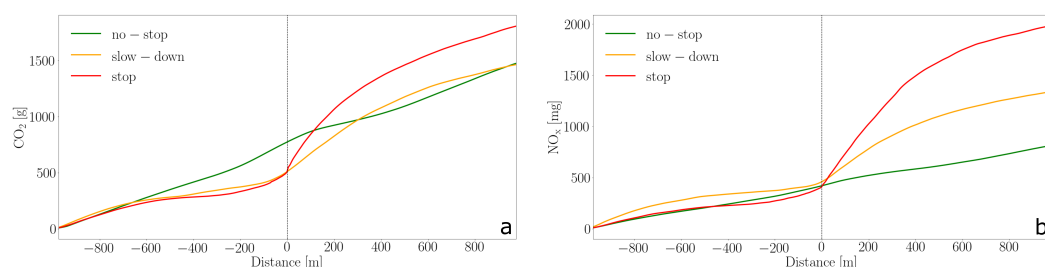


Figure 8. Cumulative flows for the three groups. Green, amber, and red represent the no-stop, slow-down, and stop groups, respectively. The position is relative to the location of the intersection as described in OSM. The vertical dashed line denotes the location of the intersection. (a) Results for the CO₂ flow for the three groups; (b) Results for NO_x for the three groups. Green, amber, and red represent the no-stop, slow-down, and stop groups, respectively.

3.4. Impact

Furthermore, 47,612 Dutch trips' speed profiles from 51 HDVs were analyzed from which 115,939 straight maneuvers while in intersection passages have been identified. The distribution of intersections per km is shown in Figure 9a. The mean of the distribution is used as a proxy to the expectation value as indicated in Equation (8), hence $\mathbb{E}[n] = 0.89$. The probabilities p_i with $i \in \{\text{no-stop}, \text{slow-down}, \text{stop}\}$ with which the three behaviors (no-stop, slow-down, stop) occur at an intersection are depicted in Figure 9b.

For this analysis, only the difference between stop and no-stop were used, which, following Equation (9), results in:

$$\Delta = s \cdot \mathbb{E}[n](p_{\text{stop}} \cdot \Delta_{\text{stop}, \text{no-stop}}), \quad (11)$$

The results for the upper bound of the yearly savings obtained by means of Equation (9) are shown in Table 3. The relative CO₂ savings were estimated using the total CO₂ emitted by HDV, also provided by CBS. The total potential CO₂ savings from HDV by means of traffic control methods is estimated at 3.2%.

Table 3. Potential energy savings from HDV in The Netherlands by using C-ITS. The first row shows the value of Δ as defined in Equation (9), that is, the yearly potential CO₂ savings, in this case for 2019. In the second row is the 2019 total CO₂ emitted by HDVs as reported by the CBS. Finally, in the third row, we show the percentage that Δ represents from the total CO₂.

Δ CO ₂ [g]	$3.58886 \cdot 10^{11}$
HDV yearly total CO ₂ [g]	$1.0756 \cdot 10^{13}$
Potential fraction saved [%]	3.2

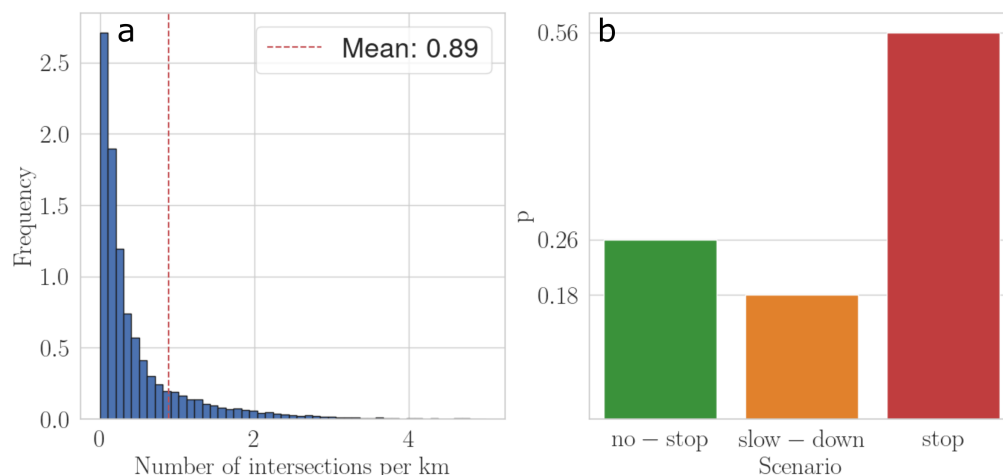


Figure 9. Values used to scale up the results to all the trips in the Netherlands. (a) The number of signalized intersections per km of road for each trip. The mean value, 0.89, represents the expectation value for the number of intersections found per km of road. (b) Shows the probabilities p_i with $i \in \{\text{no-stop, slow-down, stop}\}$ to find each of the three different behaviors when an HDV encounters a traffic light.

4. Discussion

The results indicate that avoiding a single stop in an HDV reduces NO_x emissions by 1.8 g and CO₂ emissions by 0.32 kg, saving 0.12 L of diesel fuel. As explained in Section 3, this is true for the case of optimal traffic conditions, i.e., close to free flow with minimum interaction among vehicles where the vehicles approach and leave the intersection without being affected by traffic. The cases analyzed are on the lower side of the distribution of emissions, which is not symmetrical, see Figure 6. This means that these figures underestimate the savings for each individual passage. When traffic plays a role, avoiding traffic congestion and the stop altogether would increase the savings considerably. In times of emerging C-ITS, this comes as a flexible and low-cost option for governments to improve the sustainability of freight transport reducing emissions and costs. Programming the traffic lights adequately can make the difference between being NO_x-emission compliant or not.

Due to the lack of homogeneity in the measuring methods, the different setups used and the arbitrary choice of the outcome measures, an accurate comparison of the results with other studies is not straightforward. Rough estimates can nevertheless be performed for the studies that measured trucks in naturalistic behavior. The Compass4D project reported CO₂ reductions in the range of 20 g km⁻¹ to 60 g km⁻¹ [40,41]. This is in line with the results reported in the current work, and it corresponds to the cases in which a vehicle avoids a stop every 16 km to 5.3 km. The Freilot project found aggregated levels of savings between 8% and 13% in measurements carried out over 12 months in France and the Netherlands, respectively. Based on the average distance traveled by a truck in 2012 as stated in Eurostat [55], this translates into avoiding a stop every 5 km in the Netherlands and every 8 km in France, a result that is also in line with our current findings. A previous

indication of the increase in emissions in stops has been mentioned by [56], and more recently, Özener and collaborators measured CO₂ and NO_x emissions of EURO V buses around bus stops. They indicate that around 25% and 39% of the CO₂ and NO_x emissions, respectively, are emitted in the stop areas whose length accounted for only about 9% of the route. Furthermore, they indicate that the higher number of stops in peak hours increases both CO₂ and NO_x 25% on average, which is in line with our findings.

Finally, this indicates that traffic control by means of technologies such as C-ITS could generate energy savings in the order of 3.2% of the total CO₂ generated by HDV. This estimate was computed using a large dataset, and the savings for single passages have been tested with statistical rigor. Nevertheless, the current work lacks of further detailed analysis that should follow in upcoming research. Notably, the distinction per road type could have an impact both in the emission savings and in the probabilities of finding an intersection.

Several things remain to be improved and further explored. In our analysis, the clustering focused only on the approach to the intersection. This led to the deviation of the speed profiles after the intersection to be relatively high, and furthermore, the final median speed for the different clusters is not the same. This introduces a bias in our results, making the difference between the clusters smaller. We nevertheless performed an analysis of this last part of the segments, and we found that the difference could not increase more than 0.02 km of CO₂ or 0.01 L of fuel (i.e., the 0.32 km and 0.12 L difference of CO₂ and fuel would be 0.33 kg and 0.13 L), which does not affect the main message of our work. Another important point to discuss is the increase and decrease in fuel consumption before the intersection. We hypothesize that this increase in fuel consumption (preceded by a small decrease) is of a behavioral nature. Drivers might release the throttle when approaching until they are certain that they will reach the light in green, and then they accelerate again. This is particularly relevant because it is a behavior that can be avoided with C-ITS technology that can guarantee priority to the drivers, enabling them to keep a constant speed. Finally, in the current analysis, only the speed profiles were taken into account. A detailed analysis of the vehicle's complex dynamics while approaching an intersection, also taking into account the driver's behavior, is still missing but needed for a full understanding. We encourage fellow researchers to explore that path.

5. Conclusions

The impact of signalized intersections on NO_x and CO₂ emissions in HDV was studied experimentally. It was concluded that avoiding a stop reduces the NO_x emissions in a 2 km passage by 75%. This is a key result for governments, regulatory authorities, and traffic designers to consider. Furthermore, the CO₂ levels can be reduced by 0.32 kg per intersection. This represents more than 20% of the CO₂ emitted at an intersection when stopping. Furthermore, we computed an upper bound for the total CO₂ yearly saving in the Netherlands, which resulted in 3.2% of the total CO₂ emitted by heavy duty vehicles. These figures correspond to the case in which the stop cases are replaced by no-stop cases without changing the underlying traffic conditions. If traffic flow is further improved by means of C-ITS technology, the margins would increase.

Author Contributions: Conceptualization, R.J., E.J.v.A. and N.D.; methodology, E.J.v.A. and N.D.; data analysis, E.J.v.A. and N.D.; data curation and preprocessing, R.v.G.; writing—original draft preparation, N.D. and R.v.G.; writing—review and editing, N.D. and R.v.G. All authors have read and agreed to the published version of the manuscript.

Funding: This research has been funded by the Dutch Research Council (NWO, Nederlandse Organisatie voor Wetenschappelijk Onderzoek) and TKI Dinalog as part of the CATALYST Living Lab (reference 439.18.458 A), a public private partnership that is coordinated by TNO, The Netherlands Organization for applied scientific research. This study was partially sponsored by the Metropolitan Region Rotterdam Den Haag (MRDH).

Institutional Review Board Statement: Not applicable.

Informed Consent Statement: Not applicable.

Acknowledgments: The authors want to thank the Ursa Major neo Connected Truck Trials project for making the data available. N.D. wants to thank Jessica de Ruyter for help with the dataset, Paul R. Mentink for fruitful discussions, and Norbert E. Ligterink for revising and objectively criticizing the manuscript.

Conflicts of Interest: The authors declare no conflict of interest.

Abbreviations

The following abbreviations are used in this manuscript:

ITS	Intelligent Transport Systems
C-ITS	Cooperative Intelligent Transport Systems
iTLC	Intelligent Traffic Light Controller
HDV	Heavy-Duty Vehicles
GPS	Global Positioning System
SEMS	Smart Emissions Measurement System
RPM	Revolutions per minute
EU	European Union
CBS	Central Bureau for Statistics

Appendix A

Appendix A.1. Vehicle Mass Estimation

The total mass of the vehicles (tractor and load) was estimated to have a better description of the vehicles over which the analysis was done. The calculation used Newton's second law on the power:

$$P = mva + \alpha mv + \beta v^2 \quad (A1)$$

where P is the power expressed in kW, m the total mass in t, v and a are the longitudinal velocity and acceleration in m/s and m/s², respectively, and α and β were parameters estimated on previous analysis to be $\alpha = 80 \text{ N t}^{-1}$ and $\beta = 800 \text{ N}$. These two last terms represent the rolling resistance term (assumed to be linear to the speed) and the air friction term (quadratic to the speed), respectively. The power P can be determined by means of the torque τ and the angular displacement per unit of time, this being the angular displacement $\Delta\phi$. The power is then: $P = \tau \frac{\Delta\phi}{\Delta t}$. In this case, $\Delta\phi$ is measured in RPM, hence $\Delta\phi = 2\pi\omega$ and $\Delta t = 60 \text{ s}$, which results in:

$$P = \frac{\tau 2\pi\omega}{60 \text{ s}} \quad (A2)$$

The mass distribution is shown in Figure A1, and the mean mass was 31.3 t.

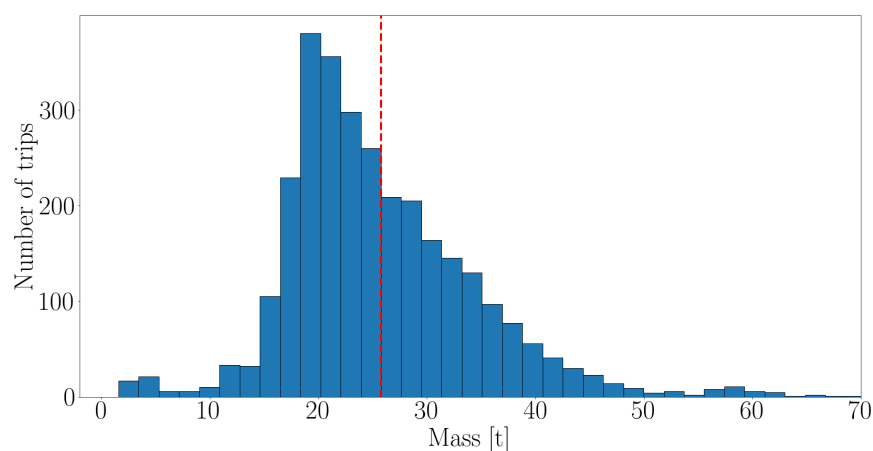


Figure A1. Distribution of the total mass of the vehicles (tractor and load). The mean value is indicated in red.

Appendix A.2. Statistical Analysis

In the need to verify whether our findings in the sample hold for the population we formulated the following null hypothesis; H_0 : The samples from each of the groups $\hat{\Xi}_j$ for $j \in \{\text{no-stop, slow-down, stop}\}$ are drawn from the same distribution. The alternative hypothesis then reads; H_A : The samples from each of the groups $\hat{\Xi}_j$ for $j \in \{\text{no-stop, slow-down, stop}\}$ are drawn from different distributions. In order to evaluate this hypothesis, several tests were performed. First, it was evaluated whether the groups were normally distributed by means of a Shapiro–Wilk test, which for both CO₂ and NO_x happened not to be the case. Hence, non-parametric statistical tests were used, namely, the Kruskal–Wallis rank sum test [57] and a Dunn pair test [58] as implemented in R [59]. The Kruskal–Wallis test indicates whether H_0 can be rejected for at least one pair of groups; if that turns true, we perform a Dunn test to find for which pair(s) of groups H_0 can be rejected or not.

Table A1 shows the results of the Kruskal–Wallis test for the CO₂. The p -value indicates that significant differences exist for a confidence level of 0.001. Furthermore, Table A2 shows the Dunn pairwise test for the CO₂. Differences between the stop group and either of the two other groups are significant for a confidence value of 0.001. This means that H_0 can be rejected in these cases, in place for the alternative hypothesis, H_A . The same procedure was performed for the NO_x values $\hat{\Theta}_j$. Tables A3 and A4 show the results for the NO_x values. In this case, for a confidence level of 0.001, we found that the null hypothesis can be rejected between the no-stop and the other two groups.

Table A1. Results of the Kruskal–Wallis test on the CO₂ showing that significant differences exist.

χ^2	Degrees of Freedom	p -Value
84.23	2	$2.2 \cdot 10^{-16}$

Table A2. Results of the Dunn pairwise test on the CO₂.

Scenario Pair	Mean Rank Difference	p -Value
slow-down \times no-stop	52.64967	0.0037
stop \times no-stop	197.80831	$2 \cdot 10^{-16}$
slow-down \times stop	145.15864	$4.7 \cdot 10^{-10}$

Table A3. Results of the Kruskal–Wallis test on the NO_x showing that significant differences exist.

χ^2	Degrees of Freedom	p -Value
142.85	2	$2.2 \cdot 10^{-16}$

Table A4. Results of the Dunn pairwise test on the NO_x.

Scenario Pair	Mean Rank Difference	p -Value
slow-down \times no-stop	141.68511	$2 \cdot 10^{-16}$
stop \times no-stop	203.46920	$2 \cdot 10^{-16}$
slow-down \times stop	61.78409	0.0019

References

- Mendoza-Villafuerte, P.; Suarez-Bertoa, R.; Giechaskiel, B.; Riccobono, F.; Bulgheroni, C.; Astorga, C.; Perujo, A. NO_x, NH₃, N₂O and PN real driving emissions from a Euro VI heavy-duty vehicle. Impact of regulatory on-road test conditions on emissions. *Sci. Total Environ.* **2017**, *609*, 546–555. [[CrossRef](#)] [[PubMed](#)]
- Liu, Y.S.; Cao, Y.; Hou, J.J.; Zhang, J.T.; Yang, Y.O.; Liu, L.C. Identifying common paths of CO₂ and air pollutants emissions in China. *J. Clean. Prod.* **2020**, *256*, 120599. [[CrossRef](#)]
- Abera, A.; Friberg, J.; Isaxon, C.; Jerrett, M.; Malmqvist, E.; Sjöström, C.; Taj, T.; Vargas, A.M. Air Quality in Africa: Public Health Implications. *Annu. Rev. Public Health* **2021**, *42*, 193–210. [[CrossRef](#)] [[PubMed](#)]

4. Cohen, A.J.; Brauer, M.; Burnett, R.; Anderson, H.R.; Frostad, J.; Estep, K.; Balakrishnan, K.; Brunekreef, B.; Dandona, L.; Dandona, R.; et al. Estimates and 25-year trends of the global burden of disease attributable to ambient air pollution: an analysis of data from the Global Burden of Diseases Study 2015. *Lancet* **2017**, *389*, 1907–1918. [[CrossRef](#)]
5. Burnett, R.; Chen, H.; Szyszkowicz, M.; Fann, N.; Hubbell, B.; Pope, C.A.; Apte, J.S.; Brauer, M.; Cohen, A.; Weichenthal, S.; et al. Global estimates of mortality associated with long-term exposure to outdoor fine particulate matter. *Proc. Natl. Acad. Sci. USA* **2018**, *115*, 9592–9597. [[CrossRef](#)]
6. Harrison, R.M.; Allan, J.; Carruthers, D.; Heal, M.R.; Lewis, A.C.; Marner, B.; Murrells, T.; Williams, A. Non-exhaust vehicle emissions of particulate matter and VOC from road traffic: A review. *Atmos. Environ.* **2021**, *262*, 118592. [[CrossRef](#)]
7. Ittmann, H.W.; King, D. State of Logistics—An overview of logistics in South Africa. In Proceedings of the CSIR 3rd Biennial Conference 2010, Science Real and Relevant, CSIR International Convention Centre, Pretoria, South Africa, 30 August–1 September 2010; p. 11.
8. Havenga, J.; Pienaar, W. Quantifying Freight Transport Volumes in Developing Regions: Lessons Learnt from South Africa's Experience During the 20th Century. *Econ. Hist. Dev. Reg.* **2012**, *27*, 87–113. [[CrossRef](#)]
9. Kaack, L.H.; Vaishnav, P.; Morgan, M.G.; Azevedo, I.L.; Rai, S. Decarbonizing intraregional freight systems with a focus on modal shift. *Environ. Res. Lett.* **2018**, *13*, 083001. [[CrossRef](#)]
10. Blauwens, G.; Vandaele, N.; de Voorde, E.V.; Vernimmen, B.; Witlox, F. Towards a Modal Shift in Freight Transport? A Business Logistics Analysis of Some Policy Measures. *Transp. Rev.* **2006**, *26*, 239–251. [[CrossRef](#)]
11. Dekker, R.; Bloemhof, J.; Mallidis, I. Operations Research for green logistics – An overview of aspects, issues, contributions and challenges. *Eur. J. Oper. Res.* **2012**, *219*, 671–679. [[CrossRef](#)]
12. Hwang, T.; Ouyang, Y. Freight shipment modal split and its environmental impacts: An exploratory study. *J. Air Waste Manag. Assoc.* **2013**, *64*, 2–12. [[CrossRef](#)]
13. Bickford, E. Emissions and Air Quality Impacts of Freight Transportation. Ph.D. Thesis, The University of Wisconsin-Madison, Madison, WI, USA, 2012.
14. Huang, Y.; Chuen Mok, W.; Shing Yam, Y.; Zhou, J.L.; Surawski, N.C.; Organ, B.; Chan, E.F.; Mofijur, M.; Mahlia, T.M.I.; Ong, H.C. Evaluating in-use vehicle emissions using air quality monitoring stations and on-road remote sensing systems. *Sci. Total Environ.* **2020**, *740*, 139868. [[CrossRef](#)]
15. Ang-Olson, J.; Ostria, S. *Assessing the Effects of Freight Movement on Air Quality at the National and Regional Level*; Office of Natural and Human Environment, US Federal Highway Administration: Washington, DC, USA, 2005.
16. Roberts, M.; Melecky, M.; Bougna, T.; Xu, Y.S. Transport corridors and their wider economic benefits: A quantitative review of the literature. *J. Reg. Sci.* **2019**, *60*, 207–248. [[CrossRef](#)]
17. van Weenen, R.L.; Burgess, A.; Francke, J. Study on the Implementation of the TEN-T Regulation—The Netherlands Case. *Transp. Res. Procedia* **2016**, *14*, 484–493. [[CrossRef](#)]
18. The European Parliament and the council of the European Union. On Union Guidelines for the Development of the Trans-European Transport Network and Repealing Decision. Regulation (EU) No 1315/2013 Official Journal of the European Union L 348, 20.12.2013. 2013. pp. 1–128. Available online: <http://data.europa.eu/eli/reg/2013/1315/oj> (accessed on 6 December 2021) [[CrossRef](#)]
19. Commission of the European Communities. Green Paper: TEN-T: A Policy Review. Towards a Better Integrated Transeuropean Network at the Service of the Common Transport Policy. 2009. Available online: <https://eur-lex.europa.eu/legal-content/en/TXT/?uri=CELEX%3A52009DC0044> (accessed on 6 December 2021).
20. Öberg, M.; Nilsson, K.L.; Johansson, C. Major transport corridors: the concept of sustainability in EU documents. *Transp. Res. Procedia* **2017**, *25*, 3694–3702. [[CrossRef](#)]
21. Conference of Europeans Directors of Roads. *Trans-European Road Network Performance Report*; Conference of Europeans Directors of Roads: Brussels, Belgium, 2017.
22. Ministry of Infrastructure and Watermanagement. *MIRT-overview, Meerjarenprogramma Infrastructuur, Ruimte en Transport (MIRT)*; Ministry of Infrastructure and Watermanagement: Hague, The Netherlands, 2020.
23. Peters, J.; McCourt, R.; Hurtado, R. Reducing carbon emissions and congestion by coordinating traffic signals. *Inst. Transp. Eng. ITE J.* **2009**, *79*, 25.
24. Barth, M.; Boriboonsomsin, K. Real-World Carbon Dioxide Impacts of Traffic Congestion. *Transp. Res. Rec. J. Transp. Res. Board* **2008**, *2058*, 163–171. [[CrossRef](#)]
25. Tully, I.M.S.N.Z. *Synthesis of Sequences for Traffic Signal Controllers Using Techniques of the Theory of Graphs*; OUEL Report; University of Oxford, Department of Engineering Science, Engineering Laboratory: Oxford, UK, 1976.
26. Guberinic, S.; Senborn, G.; Lasic, B. *Optimal Traffic Control: Urban Intersections*; CRC Press: Boca Raton, FL, USA, 2008.
27. Klein, L.A.; Mills, M.K.; Gibson, D.R. *Traffic Detector Handbook*; US Department of Transportation, Federal Highway Administration, Research, Development, and Technology, Turner-Fairbank Highway Research Center: Washington DC, USA, 2006.
28. Robertson, D.; Bretherton, R. Optimizing networks of traffic signals in real time—the SCOOT method. *IEEE Trans. Veh. Technol.* **1991**, *40*, 11–15. [[CrossRef](#)]
29. Sims, A.; Dobinson, K. The Sydney coordinated adaptive traffic (SCAT) system philosophy and benefits. *IEEE Trans. Veh. Technol.* **1980**, *29*, 130–137. [[CrossRef](#)]
30. Middleham, F. *VETAG-TEST*; Technical Report; Verkeersbureau Amsterdam: Amsterdam, The Netherlands, 1976.

31. Meyer, F. Points and Traffic Lights Under Common Control Using Vetag. *Railw. Gaz. Int.* **1975**, *131*, 193–194.
32. Ros, W. VECOM: A powerful local communication channel between vehicle-borne and roadside systems. In Proceedings of the ESA Workshop on Land Mobile Services by Satellite, Noordwijk, The Netherlands, 3–4 June 1986; pp. 23–25.
33. Festag, A. Cooperative intelligent transport systems standards in europe. *IEEE Commun. Mag.* **2014**, *52*, 166–172. [[CrossRef](#)]
34. Roess, R. *Traffic Engineering*; Pearson: Upper Saddle River, NJ, USA, 2011.
35. Chang, D.J.; Morlok, E.K. Vehicle Speed Profiles to Minimize Work and Fuel Consumption. *J. Transp. Eng.* **2005**, *131*, 173–182. [[CrossRef](#)]
36. Wang, J.; Rakha, H.A. Fuel consumption model for heavy duty diesel trucks: Model development and testing. *Transp. Res. Part Transp. Environ.* **2017**, *55*, 127–141. [[CrossRef](#)]
37. Guardiola, C.; Pla, B.; Pandey, V.; Burke, R. On the potential of traffic light information availability for reducing fuel consumption and NO_x emissions of a diesel light-duty vehicle. *Proc. Inst. Mech. Eng. Part D J. Automob. Eng.* **2019**, *234*, 981–991. [[CrossRef](#)]
38. Meneguzzer, C.; Gastaldi, M.; Rossi, R.; Gecchele, G.; Prati, M.V. Comparison of exhaust emissions at intersections under traffic signal versus roundabout control using an instrumented vehicle. *Transp. Res. Procedia* **2017**, *25*, 1597–1609. [[CrossRef](#)]
39. Koenders, E. FREILOT. Urban Freight Energy Efficiency Pilot. D. FL. 3.1 Final Operation Report. 2012. Available online: <https://cordis.europa.eu/docs/projects/cnect/0/238930/080/deliverables/001-DFL31Finaloperationreportv10.pdf> (accessed on December 6 2021).
40. Mitsakis, E.; Salanova Grau, J.M.; Aifandopoulou, G.; Tona, P.; Vreeswijk, J.; Somma, G.; Blanco, R.; Alcaraz, G.; Jeftic, Z.; Toni, A.; et al. Large scale deployment of cooperative mobility systems in Europe: COMPASS4D. In Proceedings of the 2014 International Conference on Connected Vehicles and Expo (ICCVE), Vienna, Austria, 3–7 November 2014; pp. 469–476. [[CrossRef](#)]
41. Vreeswijk, J.; Vernet, G.; Huebner, Y.; Jeftic, Z.; Tona, P.; Martinez, J.M.; Mitsakis, E.; Alcaraz, G. Compass4d: Cooperative mobility pilot on safety and sustainability services for deployment. In Proceedings of the 10th ITS European Congress, Helsinki, Finland, 16–19 June 2014.
42. Agarwal, A.K.; Mustafi, N.N. Real-world automotive emissions: Monitoring methodologies, and control measures. *Renew. Sustain. Energy Rev.* **2021**, *137*, 110624. [[CrossRef](#)]
43. van Kempen, E.; de Rooter, J.; Souman, J.; van Ark, E.J.; Deschle, N.; Oudenes, L.; Geurts, M.; van der Horst, R.; Janssen, R.; Dinalog, T. *Real-World Impacts of Truck Driving with Adaptive Cruise Control on Fuel Consumption, Driver Behaviour and Logistics*; Report Number 10516; TNO Publications, The Hague, The Netherlands 2021. Available online: <https://repository.tudelft.nl/islandora/object/uuid%3A7bd21500-957a-492d-ad42-4d3c22d55a37> (accessed on 6 December 2021).
44. Kadijk, G.; Ligterink, N.; Spreen, J. On-Road NO_x and CO₂ Investigations of Euro 5 Light Commercial Vehicles 2015. Report Number 10192; TNO Publications: The Hague, The Netherlands. Available online: <https://repository.tno.nl/islandora/object/uuid:d212320e-7b4c-4440-ae93-3dfe386c9dec> (accessed on 6 December 2021).
45. Vermeulen, R.J.; Ligterink, N.E.; Vonk, W.A.; Baarbé, H.L. A Smart and Robust NO_x Emission Evaluation Tool for the Environmental Screening of Heavy-Duty Vehicles. In Proceedings of the 19th International Transport and Air Pollution Conference 2012, Thessaloniki, Greece, 26–27 November 2012; pp. 1–11.
46. Kadijk, G.; Vermeulen, R.; Buskermolen, E.; Elstgeest, M.; van Heesen, D.; Heijne, V.; Ligterink, N.; van der Mark, P. *NO_x Emissions of Eighteen Diesel Light Commercial Vehicles: Results of the Dutch Light-Duty Road Vehicle Emission Testing Programme 2017*; TNO: Delft, The Netherlands, 2017; R11473.
47. Heepen, F.; Yu, W. *SEMS for Individual Trip Reports and Long-Time Measurement*; SAE Technical Paper Series; SAE International: Warrendale, PA, USA, 2019. [[CrossRef](#)]
48. Luxen, D.; Vetter, C. Real-time routing with OpenStreetMap data. In Proceedings of the 19th ACM SIGSPATIAL International Conference on Advances in Geographic Information Systems (GIS '11), Chicago IL, USA, 1–4 November 2011; ACM: New York, NY, USA, 2011; pp. 513–516. [[CrossRef](#)]
49. OpenStreetMap Contributors. Planet Dump Retrieved from. 2020. Available online: <https://www.openstreetmap.org>; <https://planet.osm.org> (accessed on 6 December 2021).
50. Maurya, A.K.; Bokare, P.S. Study of Deceleration Behaviour of Different Vehicle Types. *Int. J. Traffic Transp. Eng.* **2012**, *2*, 253–270. [[CrossRef](#)]
51. Ligterink, N.E. *On-Board Determination of Average Dutch Driving Behaviour for Vehicle Emissions*; TNO: Utrecht, The Netherlands, 2016; R10188.
52. Centraal Bureau voor de Statistiek. Available online: <https://www.cbs.nl/> (accessed on 6 December 2021).
53. Council of European Union. Council Regulation (EU) No 595/2009. 2009. Available online: <https://eur-lex.europa.eu/legal-content/EN/TXT/?uri=CELEX:02009R0595-20200901> (accessed on 6 December 2021).
54. Council of European Union. Council regulation (EU) No 582/2011. 2011. Available online: <https://eur-lex.europa.eu/legal-content/EN/TXT/?uri=CELEX:02011R0582-20180722> (accessed on 6 December 2021).
55. Eurostat. Summary Of Annual Road Freight Transport By Type Of Operation And Type Of Transport. 2012. Available online: https://ec.europa.eu/eurostat/databrowser/product/view/ROAD_GO_TA_TOTT (accessed on 6 December 2021).
56. Clark, N.N.; Kern, J.M.; Atkinson, C.M.; Nine, R.D. Factors Affecting Heavy-Duty Diesel Vehicle Emissions. *J. Air Waste Manag. Assoc.* **2002**, *52*, 84–94. [[CrossRef](#)]
57. Kruskal, W.H.; Wallis, W.A. Use of ranks in one-criterion variance analysis. *J. Am. Stat. Assoc.* **1952**, *47*, 583–621. [[CrossRef](#)]
58. Dunn, O.J. Multiple comparisons among means. *J. Am. Stat. Assoc.* **1961**, *56*, 52–64. [[CrossRef](#)]
59. R Core Team. *R: A Language and Environment for Statistical Computing*; R Foundation for Statistical Computing: Vienna, Austria, 2017.